Assessment of vulnerability to erosion: digital mapping of a loess cover thickness and stiffness using spectral analysis of seismic surface-waves

Kevin Samyn, Olivier Cerdan, Gilles Grandjean, Romain Cochery, Séverine Bernardie, Adnand Bitri

Assessment of vulnerability to erosion: digital mapping of a loess cover thickness and stiffness using spectral analysis of seismic surface-waves

K. Samyn[1], O. Cerdan[1], G. Grandjean[1], R. Cochery[1], S. Bernardie[1], A. Bitri[1]*

(1) BRGM, Risks Department, 3 Avenue Claude Guillemin, BP36009 45060 Orléans Cedex 2, France

** Corresponding author. BRGM, Risks Department, 3 Avenue Claude Guillemin BP36009 45060 Orléans Cedex 2, France. Tel.: +33 (0)2 38 64 34 54; fax: +33 (0)2 38 64 36 89. E-mail address: k.samyn@brgm.fr (K. Samyn).*

Abstract

Non-invasive geophysical techniques offer an interesting alternative to traditional soil sampling methods, especially for estimating spatial variations of soil parameters in the landscape. The spectral analysis of seismic surface-waves (*MASW*) can be used to determine the vertical shear-wave velocity (*Vs*) model (i.e., vertical variations in *Vs* with depth). In our study, MASW soundings were determined at each point in a grid spread over *a* wind-eroded field plot of 15600 m^2. *Vs* was then mapped in terms of the thickness and stiffness of the superficial loamy material horizon, which are called *ThickLM* and *StiffLM, respectively*. To relate the *Vs* values to the soil stiffness, cone resistance (*Qd*)

soundings were also performed using a Dynamic PANDA penetrometer. Concurrently, boreholes were used to sample the same horizon for bulk soil density (ρ_b) measurements. Based on these measurements, large variations in *ThickLM* were observed. The distribution of *Vs* values along a 130 m transect allowed for the distinction between two layers corresponding to different mechanical properties. The *Vs* value of 240 m/s was then used as a limit between the loamy material and the underlying clays. This limit was validated using drilling observations performed on the same transect. Therefore, it was possible to map the *ThickLM,* which varied between 0.2 and 6.5 m over the entire field. The comparison between the averaged values of *Vs* and *Qd* in the loamy material layer showed a significant correlation (R^2=0.4) such that the mapping of *StiffLM* was realised from the *Vs* map and the *Vs-Qd* relationship. Density comparison between the ρ_b measured on drill samples and the ρ_b calculated from *Vs* were also performed using previously published relationships; however, significant correlations were not observed. The obtained maps of *ThickLM* and *StiffLM* were consistent with the expected effects of erosion at the catchment scale and provide indications of historical erosion events. This methodology, which provides a structural and mechanical characterisation of subsurface materials, should help to focus conservation measures to the most threatened areas (i.e., the identification of areas that show a reduced *ThickLM* and increased *StiffLM,* which are associated with high soil erosion vulnerability and/or high compaction state).

Keywords

Surface wave; Erosion; Digital mapping; Shear wave velocity; Cone resistance

1. Introduction

The current growing awareness of ecological issues has led to an increasing demand for environmental datasets that are necessary for adequate monitoring and management of various threatened ecosystems. There is also a growing concern regarding the sustainability of biomass production, not only in developing or semi-arid areas (Hadgu et al., 2009; Ye and Van Ranst, 2009) but also in industrialised countries. The increasing demand for cereals and biofuels will further accentuate this trend. Strong relationships between soil erosion, soil depth and soil productivity have been reported in various environments (e.g., Biot and Lu, 1995; Tendberg et al., 1997; Heckrath et al., 2005; Rejman and Iglik, 2010). The regolith and, more generally, the soil surface material are particularly important, as they support human activities and fulfil numerous ecosystem services (European Commission., 2002-2006). However, our knowledge of the nature and spatial extent of surficial materials is far from complete, and therefore further research is necessary to fill this gap. The ability to accurately and rapidly produce soil depth maps or to delineate areas with

limited root penetration depths will, therefore, become crucial to address these issues. Conventional soil surveys are generally based on manual sampling and visual observations of soil pits or auger holes. Such observations are met with both methodological and economic constraints when used for the investigation of large areas. Not only are these observations extremely time consuming – and thus costly – because of the highly repetitive fieldwork that is needed, they can also be destructive to the soil. Moreover, this type of local observation may not represent larger-scale trends in soil properties.

Geophysical techniques offer an interesting alternative to traditional soil sampling methods, especially for estimating the spatial variability of physical soil parameters of large areas. These techniques are particularly relevant because most physical soil characteristics are closely related to soil properties (e.g., geo-electrical properties) (Rhoades and van Schilfgaarde, 1976; Robain et al., 1996; Samouëlian et al., 2005). For example, a significant correlation has been demonstrated between the apparent electrical resistivity (ρ) or electrical conductivity (σ) and the soil texture (Williams and Hoey, 1987), soil water content (Kachanoski et al., 1988; Kalinski and Kelly, 1993; Michot et al., 2003), soil salt or nutrient content (Rhoades and Corwin., 1981; Eigenberg et al., 1998) or soil depth (Thompson and Bell., 1996; Chaplot et al., 2001). In contrast to these electrical methods, seismic techniques are not well established in soil sciences but could be particularly promising. Due to the development of subsurface characterisation studies for environmental or geotechnical purposes,

the efficiency of seismic methods for estimating ground velocity structures and mechanical properties has seen considerable progress in the recent decades and has been used in various applications in several fields: waste disposal (Lanz et al., 1998), landslides (Grandjean et al., 2007), or hydrogeophysics (Sturtevant et al., 2004). Modern equipment, which generally features 48 or 72 recording channels and PC-piloted acquisition software, has made this method user-friendly and has contributed to its popularity. Recently, an adaptation of the sensor line, which is based on unplugged gambled geophones, was proposed to drastically reduce the acquisition times (Grandjean, 2006a; Debeglia et al., 2006). This improvement was supported by the development of new data processing protocols, such as acoustical tomography (Azaria et al., 2003; Grandjean, 2006b) or spectral analysis of surface-waves (SASW) (Nazarian et al., 1983; Park et al., 2000; Grandjean and Bitri, 2006) and related multichannel MASW applications (Foti, 2000; Miller, 1999; Park et al., 1999a, 1999b; Xia et al., 1999), which allowed for the construction of shear waves velocity (Vs) profiles. For example, the analysis of fundamental-mode Rayleigh waves is one of the most common methods for using the dispersive properties of surface waves (Bullen, 1963). This type of analysis provides essential parameters that are commonly used to evaluate near-surface stiffness, which is a critical property for many geotechnical studies (Stokoe et al., 1994). SASW uses the spectral analysis of the ground roll that is generated by an impulsive source and is recorded by a pair of receivers. This method has been widely and effectively

112 used in many geotechnical engineering projects (Stokoe et al., 1994). A single
113 pair of receivers is configured and reconfigured (based on wavelength
114 calculations made during the acquisition) as many times as necessary to
115 sample the desired frequency range. Unfortunately, the necessity of recording
116 repeated shots during multiple field deployments for a given site increases the
117 time and labour requirements relative to a multichannel procedure. Multichannel
118 analysis of surface waves (MASW) is designed to overcome the few
119 weaknesses of the SASW method. The purpose of this study is to test the
120 MASW method as a new tool for characterising soil mechanical properties (i.e.,
121 soil thickness and stiffness) with respect to erosion processes.
122 Instead of sounding the area by systematic drilling, seismic methods were
123 tested to efficiently produce soil property maps. Specifically, we evaluated the
124 feasibility of using mechanical contrasts that exist between the lithologies to
125 map the thickness and stiffness (*ThickLM* and *StiffLM,* respectively) of the
126 surface loamy material horizon using Vs data. Based on this process, we should
127 be able to identify the most threatened areas at the catchment scale, i.e., areas
128 that show a reduced *ThickLM* associated with high *StiffLM*, using *Vs* data
129 coupled to cone resistance (*Qd*) data because *StiffLM* can be used as a
130 surrogate for the soil erodibility.
131

132 **2. Materials and methods**

133

134 *2. 1. Description of the study field*

135

136 The study area was located within the Bourville catchment in Normandy, a
137 region of Northern France where erosion that removes the upper soil horizons is
138 a major threat to the main soil functions (i.e., “food and other biomass
139 production, storage, filtering, and transformation of elements among which
140 water and nutrients, biological habitat, and source of raw materials”, European
141 Commission, 2002; Van-Camp et al., 2004). The studied area includes a
142 catchment of the European loess belt in Normandy; this region is severely
143 affected by water and wind erosion with rates often exceeding soil production
144 (between 5 and 10 $ton.ha^{-1}.yr^{-1}$; Cerdan et al., 2010) (Figure 1). Normandy has
145 a humid-temperate climate with few days of frost. The average temperature
146 ranges between 10 and 12 °C throughout the year, and in August, which is the
147 hottest month of the year, the temperature fluctuates approximately 18 °C. The
148 hilly areas, characterised by a smooth relief (0-7%) and deep superficial layer
149 (>5 m), are used for intensive production of alternating winter and spring crops
150 (e.g., wheat, beets, and maize). An area of approximately 1.5 ha was selected
151 in this catchment to test our approach. Not only was this area highly degraded
152 with a quasi-complete removal of the soil cover in certain areas, its surrounding
153 areas also showed a gradation in the thickness of the loamy material horizon
154 from thick and well conserved in the low elevation locales to thin and eroded in
155 the high elevation areas. The research plot was delineated within the transition

156 zone. This plot, which extended along the steepest slope (Figure 1), shows
157 clear evidence of soil degradation in its north-west and south-east areas with
158 the presence of outcropping clays with flints, both of which are characteristics of
159 on-going loamy material horizon erosion. The entire soil surface was covered by
160 grass vegetation during the field study.
161
162 *2. 2. Geological setting and geomorphologic conditions*
163 The study area was located in north-western France (Normandy), which is
164 characterised by a humid-temperate climate. The topography was relatively
165 smooth with slope gradients ranging between 1% and 4% on the plateau and
166 4% to 10% on valley sides. The area is covered by silt loam soils, which
167 developed on the loess Quaternary deposit, and contains at least 60% silt in the
168 surface horizons. These soils are classified as Neoluvisol in the French
169 Classification system and are described as 'excessively drained' according to
170 the USDA (2003) soil drainage classification (Orthic Luvisol, World Reference
171 Base, 1998). Such soils are very sensitive to soil sealing because of their low
172 clay content (130 to 170 $g.kg^{-1}$) and low organic matter content (10 to 20 $g.kg^{-1}$)
173 relative to more competent underlying clays that are enriched with flints. When
174 in arable use, large areas are left bare and open to rainfall during most of the
175 cultural season, which, combined with the sensitivity to sealing, renders them
176 vulnerable to runoff and water erosion (Figure 2). In contrast, sediments
177 accumulate due to erosion flows in sheltered areas. Based on the

178 geomorphologic conditions, the thickness of the uppermost loamy sediments
179 presents a high variability at the catchment scale.
180
181 *2. 3. Theory and basic principles of the MASW method*
182
183 In the majority of surface seismic surveys, when a compressional wave source
184 is used, more than two-thirds of the total seismic energy generated is imparted
185 into Rayleigh waves (Richart et al., 1970), which is the principal component of
186 surface waves. Assuming vertical velocity variation, each frequency component
187 of a surface wave has a different propagation velocity (called the phase velocity,
188 *Cf*) at each unique frequency (*f*) component. This unique characteristic results
189 in a different wavelength (*λf*) for each frequency that is propagated. This
190 property is called dispersion. Although surface waves are considered noise in
191 body-wave surveys (i.e., reflection or refraction profiling), their dispersive
192 properties can be used to infer near-surface elastic properties via Vs evaluation
193 (Nazarian et al., 1983; Stokoe et al., 1994; Park et al., 1998a). The entire
194 process typically used to produce reliable Vs profiles via the spectral analysis of
195 surface waves involves three steps: (1) the acquisition of surface waves (Figure
196 3,5a), (2) the construction of dispersion curves (a plot of phase velocity as a
197 function of *f*) (Figure 5b), and (3) the back calculation (inversion) of the Vs
198 profile from the calculated dispersion curve (Figure 5c,d). A workflow diagram

199 illustrating the processing method used to obtain reliable Vs profiles with depth
200 is presented in Figure. 4.
201 For step (1), to obtain a good estimation of dispersion curves, we used a multi-
202 station (MASW) configuration, in which receivers are set at several locations
203 and are regularly spaced along a straight line. A seismic source signal was
204 generated via the impact of a hand-held hammer hitting a small iron anvil
205 located on the ground. During the recording, the wavefield was discretised and
206 truncated in both the time and space domain (Figure 5a). The sampling periods
207 in the time domain were *Dt=0.5 ms*; the numbers of samples was *M=1000.* The
208 near offset (also called origin offset; i.e., the distance between the source point
209 and the first recording point along the line) of x_0*=50 cm*, the geophone spacing
210 of *Dx=50 cm* and the offset range of *L=11.5 m* (Figure 3) are the three important
211 acquisition parameters that require proper selection to prevent aliasing, near
212 field, and far field effects (Xia et al., 1999 and Miller et al., 1999). These effects
213 determine the minimum and maximum depth in which *Vs* can be accurately
214 measured using the *MASW* method. Due to certain undesirable effects,
215 Rayleigh waves must be studied beyond the near field offset. Far from this
216 distance, they can be considered as horizontally travelling plane waves and
217 processed accordingly. The adaptation of *MASW* to soil investigations is first
218 conditioned by the possibility of reducing the seismic array (originally consisting
219 of several tens of meters) to approximately several meters, provided that near-
220 field effects are avoided. Second, the frequency range of the seismic signal is

221 increased to obtain a depth of interest up to a maximum of 10 m below the
222 ground surface. Finally, the selected seismic system involved a hammer source
223 that was capable of generating signals in the 1 to few tens of Hz frequency
224 range; and a seismic antenna composed of 24 geophones capable of recording
225 signals from 10 to 200 Hz was used. The entire system was towed behind a
226 vehicle (Figure 3a) to ensure a rapid acquisition. A total of 157 seismic
227 observations were performed along 13 transects with regular 12 m spaces
228 between data points, as shown in Figure 1.
229 For step (2), the generation of a dispersion curve is one of the most critical
230 steps for generating an accurate Vs profile. Dispersion curves are generally
231 displayed as *Cf* as a function of *f* (Figure 5b). For impulsive data, a frequency-
232 domain approach (Park et al., 1998b) is used to calculate the dispersion curve.
233 This approach involves a 2D wavefield operation that transforms seismic data
234 from the space-time domain into the *Cf-f* domain, which is more convenient for
235 highlighting dispersion features.
236 For step (3), the Vs profiles were calculated using an iterative inversion process
237 (Tarantola, 1987) that requires dispersion data (Figure 5c). A least-squares
238 approach allows for the automation of the process (Xia et al., 1999). For the
239 method used here, only the Vs and model thickness are updated after each
240 iteration; Poisson's ratio remains unchanged throughout the inversion. An initial
241 earth model needed to be specified as a starting point for the iterative inversion
242 process. The earth model consists of velocity (*P*-wave and *S*-wave velocity),

density, and thickness parameters. Among these four parameters, Vs has the most significant effect on the reliable convergence of the algorithm. For each iteration of the inversion process, an update of Vs is calculated, and synthetic dispersion curves are back calculated from this new Vs model. The synthetic dispersion curve is then compared to the observed dispersion curve based on the least-squares method (Figure. 5d). A reliable Vs model is obtained when the misfit between synthetic and observed dispersion curves is minimised. The inversion algorithm used in our study implements all of these aspects and is based on Hermann (1987). The stop criterion for the *Cf* residuals between synthetic and observed dispersion curves was defined as less than 5 $m.s^{-1}$. Finally, the interpolation of contiguous *Vs* models resulting from the inversion process is realised using a natural neighbour method to obtain a 2D *Vs* section along the transect.

2. 4. Penetrometer soundings

A dynamic penetrometer with variable energy (Afnor, French norm NF XP P 94-105) can be used to record the mechanical resistance (*Qd* in MPa) variation with depth (Sanglerat, 1975; Burns and Mayne, 1996) by manually driving a rod into the soil using a standardised hammer. Therefore, a penetrometer can be used to identify variations in soil profiles according to the penetration modulations observed on the rod at each blow of the hammer. Because this

method is easy to use and relatively quick, this portable automatic penetrometer is well adapted for detailed prospecting and mapping (Zhou, 1997). Each penetrometric sounding (CPT) products a vertical cone resistance profile called a penetrogram; the interpretation of the penetrogram allows for the identification of different layers and that estimation of their thickness using two main criteria: well-defined cone resistance thresholds and the shape of the penetrogram. *Qd* is calculated using the following relationship (Langton, 1999):

$$Qd = \frac{1}{A} \times \frac{\frac{1}{2} MV^2}{e} \times \frac{1}{1 + \frac{P}{M}} \qquad (1)$$

where A is the cone section (2 cm^2), M is the striking mass (kg), V is the impact velocity (ratio between the cell spacing and travel time between cells), P is the struck mass (kg) and e is the drill string progress (m). *Qd* soundings were performed using a Dynamic PANDA penetrometer (Gourvès and Barjot, 1995) along transect n°5 of the field plot with a regular spacing of 12 m; this survey was conducted at the same location as the collection of seismic data points (Figure 1). In this study, we assimilated the cone mechanical resistance *Qd* into the soil stiffness.

2. 5. Drilling observations

In addition to the abovementioned surveys, 4 drilling observations were performed on the same transect with a spacing of 40 m in the midslope and 20 m in the footslope regions (Figure 1). Each borehole was excavated in the north-west to south-east direction to depths of 1.85 m, 3.5 m, 6 m and 1.7 m. Drilling cores were used to estimate *ThickLM* and for laboratory measurements of the water content (θ), the real density of the solid (ρ_r) and the bulk density (i.e., the density of the sample as a whole) (ρ_b) in the loamy layer; these results are shown in Table 1.

2. 6. Sensitivity of Vs to soil mechanical properties

Numerical relationships between soil mechanical properties and Vs have been previously published. One of these relationships, which is given by elastic theory and is an essential property for evaluating dynamic responses and the stiffness of soil, is the small-strain shear modulus, G (i.e., a measure of solidity). Values of G are typically determined indirectly by measuring the shear wave velocity, Vs, and the mass density of the soil, ρ, and computing $G= \rho Vs^2$. Other commonly used relationships include the correlation between cone penetration resistance or SPT blow count (N) and Vs and functional forms; this relationship is reported to be $Vs=A.N^S$, where the constants A and B are determined by a statistical regression of a data set. A significant number of correlations have

been published for various soil types. Imai and Yoshimura (1975) studied the relationship between seismic velocities and certain index properties for 192 samples and developed empirical relationships for all soil types. Sykora and Stokoe (1983) reported that geological age and type of soil are not predictive of Vs, whereas the uncorrected SPT-N value is the most important term. Sykora and Koester (1988) demonstrated a strong statistical correlation between the dynamic shear resistance and standard penetration resistance of soils. Iyisan (1996) examined the influence of the soil type on the correlation between SPT-N and Vs using data collected from an earthquake-prone area in the eastern part of Turkey. The results showed that with the exception of gravels, the correlation equations developed for all soils, sand and clay yield approximately similar Vs values. Jafari et al. (2002) presented a detailed historical review of the statistical correlation between SPT-N and Vs. Hasancebi and Ulusay (2006) studied similar statistical correlations using 97 data pairs collected from an area in the north-western part of Turkey and developed empirical relationships for sands, clays, and all soils irrespective of soil type. Ulugergerli and Uyanık (2007) investigated statistical correlations using 327 samples collected from different areas of Turkey and defined the upper and lower bounds of an empirical relationship instead of a single average curve for estimating seismic velocities and relative densities.

These previous studies, as well as a qualitative comparison of data available on our study site, demonstrate the good correlation of Vs to soil mechanical

properties and allow for the expectation of a relatively good characterisation of StiffLM using Vs and an accurate estimation of ThickLM (Figure 6) in this context.

3. Evaluation of ThickLM and StiffLM of the loamy material horizon

3. 1. Relationships between Vs and CPTs

The distribution of *Vs* values inverted along the transect n°5 allowed for the discrimination between two populations that corresponded to different mechanical properties. Each population was characterised by Gaussian laws of $mean_{1st\ layer}$ = 171 $m.s^{-1}$, $\sigma_{1st\ layer}$ = 80 $m.s^{-1}$and of $mean_{2nd\ layer}$ = 347 $m.s^{-1}$, $\sigma_{2nd\ layer}$ = 76 $m.s^{-1}$, where σ is the standard deviation (Figure 7). Moreover, the isovalue of *Vs*=240 $m.s^{-1}$ was highly consistent with the isovalue Qd=20 MPa, which marks the boundary between a soft superficial unit and a competent underlying formation (Figure 8). This observation was then used for the calibration of a Vs threshold value (VsLim = 240 $m.s^{-1}$) to characterise a mechanical limit used as a criteria to map ThickLM over the entire field based on the entire seismic dataset. Finally, the mean squared error (MSE) between ThickLM observations and estimations were computed using a validation set of 4 drilling points that were positioned to be representative of the observed main variability of ThickLM.

To study the stiffness of the loamy material-horizon, we compared Vs and Qd, obtained by CPTs, at a same depth. The two parameters can be interrelated because they are both influenced by effective level of confining stress, the anisotropic K_0-stress state, mineralogy, aging, bonding, and other factors (Mayne and Rix, 1995; Stuedlein, 2010; Dikmen, 2009). We first applied an exclusion filter to the *Vs* data with the condition *Vs* < VsLim to restrict the analysis to the loamy layer. Then, we computed the average *Qd* values in each interval of Vs 1D models. Nugget effects on the *Qd* data, which occur due to the punctual presence of various defects (e.g., pebbles) in the medium, were previously removed from the dataset using an interpolating operator. Figure 9 shows the linear regression between Vs and Qd where a correlation between *Qd* and e^{Vs} is observed whith R^2=0.4 and a two-tailed P value less than 0.0001. By conventional criteria, this difference is considered to be extremely statistically significant even if samples are highly scattered. Therefore, we predicted *Qd* according to *Vs* using the following equation:

$$Qd = 1.2965e^{0.0057Vs} \qquad R^2 = 0.4 \qquad P < 0.0001 \qquad (2)$$

Mapping of the spatial variation of *StiffLM* as a function of the average *Qd* calculated over *ThickLM* using Eq. (2) then becomes possible over the entire field. Density comparisons between the ρ_b measured for the drill samples and the ρ_b calculated from *Vs* using published relationships (Mayne, 2001) were

372 also performed, and no significant correlations were determined. This absence
373 of correlations was probably due to the lack of ρ_b values for the clay formation.
374
375 *3. 2. Spatial structure and interpolation of the data*
376
377 The spatial structures of *ThickLM* and *StiffLM* were assessed using variograms
378 that were estimated in four directions at 20°, 55°, 110° and 155° from
379 geographic north. The variograms were generated using all possible sample
380 pairs in a given direction and by grouping these into classes (lags) of
381 approximately equal distance (Matheron, 1965). The variances (one-half of the
382 mean squared difference) of these paired sample measurements were then
383 plotted as a function of the distance between samples to provide a means of
384 quantifying the spatial structure of the data. *ThickLM* and *StiffLM* obtained using
385 *MASW* and Eq. (2), respectively, were then interpolated using ordinary kriging.
386 Ordinary kriging is a geo-statistical method that takes into account both the
387 distance and the degree of variation between known data points and relies on
388 the spatial correlation structure of the data to determine the weighting values.
389 This type of kriging has been shown to provide better performance for soil
390 parameters than other available methods (e.g., Burgess et al., 1981; Myers,
391 1994). The interpolations were accomplished by fitting each of several
392 theoretical variogram models (i.e., linear, Gaussian, spherical, and exponential
393 models) to the empirical isotropic variogram using the least-squares method.

The best fit model was then used for the interpolation. Data points were subsequently interpolated to a regular 2×2 m grid using a full second-order polynomial drift function, which is the common practice.

4. Results

ThickLM ranged between 0.2 and 6.5 m with an average of 2.6 m and a median of 2.7 m (Table 2; Figure 10a). As shown by the variogram analysis (Figure 11a), *ThickLM* exhibited a moderate anisotropy and spatial structure. Nevertheless, a slight azimuth dependence of less and greater variability was observed at the the 20° and 110° directions, respectively, relative to the other directions of less and greater variability than the other directions. The observations were interpolated over the 120×130 m plot and using an exponential model (sill = 0.75; range = 4.5 m) coupled with a Gaussian model (sill = 9; range = 70 m). The interpolated *ThickLM* map showed a gradual increase in thickness from the north-west limit of the plot, where values were approximately 0.20 m, to the mid-plot position; a gradual decrease was then observed from the mid-plot position to the south-east limit, where *ThickLM* was approximately the same as on the north-west side (Figure 10a). An area of greater *ThickLM* (between 3 and 6.5 m) was observed at the mid-plot position. A local area of greater *ThickLM* (between 1.5 and 3 m) was observed on the north-west side of the plot. The differences between the observed and

estimated ThickLM values are shown in Figure 12. The MSE of 0.043 m and R^2=0.956 between these two variables over the 4 validation points shows that the estimated ThickLM could be considered to be accurate based on the consideration that the drilling observations are determined to be representative of the overall observed variability of ThickLM over the entire plot.

StiffLM, which is related to the mean *Qd* calculated over *ThickLM,* ranged between 2 and 6 MPa with an average of 3.78 MPa and a median of 3.68 MPa (Table 2; Figure 10b). As demonstrated by the variogram analysis (Figure 11b), *StiffLM* exhibited a moderate anisotropy and spatial structure. Anisotropy was observed between the 20 and 110° directions with less and greater variability than the other directions. The observations were interpolated over the 120×130 m plot using a Gaussian model (nugget = 0.1; sill = 0.7; range = 50 m). The interpolated *StiffLM* map showed a gradual decrease in stiffness from the north-west limit of the plot, where the values range between 5 and 6 MPa, to the mid-plot position; a gradual increase from mid-plot position to the south-east limit, where *StiffLM* presented an lower stiffness than on the north-west side, was also observed (Figure 10b). An area of lower *StiffLM* (between 2 and 4 MPa) was observed at the mid-plot position. A local zone of lower *StiffLM* (approximately 4 MPa) was observed in the north-west side of the plot.

5. Discussion

The maps of *ThickLM* and *StiffLM* were in good agreement with the expected consequences of the on-going erosion of the loamy material horizon: a gradation in the thickness of the loamy material-horizon from thick and well conserved in the lower parts to thin and eroded in the upper parts, was observed (Figure 10a). The increase of *StiffLM* at the limits of the study plot shows clear evidence of soil degradation in the north-western and south-eastern zones with the presence of bare soils and outcropping clays and flints, which have a mechanical resistance. The local event of greater *ThickLM* and lower *StiffLM* indicated on Figures 10a and 10b with a black dotted line should correspond to a buried former gully that was photographed at this location 2 years prior to the study and was caused by strong runoff activity (Figure 10c). This structural and mechanical characterisation of the loamy material horizon should not only help to focus conservation measures in the most threatened areas (i.e., areas that show a reduced *ThickLM* and increased *StiffLM* associated with high soil erosion vulnerability and/or a high compaction state), but will also help identify historical erosion events. The combination of maps of soil stiffness and surficial sediment depths will allow the development and implementation of soil conservation measures to target high-priority areas. Where climatic scenarios are available, these maps can also be used to calculate the potential productivity loss using simulators, such as the SimPLE.ca model (Bremer et al., 2008). This method will also contribute to the broad discussion of reducing the inherent uncertainty in current soil mapping or

attribute determinations. Soil maps show that there can be considerable uncertainty in map unit composition with resulting spatial variability in soil properties within map units (Webb and Lillburne, 2005). Actual soil maps define discrete soil classes, which represent the interpolation of only a limited number of modal soil profiles without capturing the full extent of soil variability (Campbell and Edmonds, 1984; Qi and Zhu, 2011). In the study presented here, the non-destructive mapping of continuous soil properties in space will help to improve the data frequency and allow for the derivation of probability distributions to parameterise the fuzzy nature of the geographical objects that comprise the soil maps (Martin-Clouaire et al., 2000).

6. Conclusions

The objective of this study was to test and validate a new geophysical technique for mapping soil properties that are related to soil erosion processes. A seismic experiment coupled with penetrometric measurements form the basis of the proposed methodology. The MASW method was efficient for producing Vs models over large areas. When coupled with penetrometric measurements of Qd variations with depth, high-resolution maps of soil thickness and stiffness

481 can be produced, provided that a correlation is found to occur between Vs and
482 Qd.
483 We demonstrated that accurate mapping of variations in the thickness and
484 stiffness of the loamy material horizon can be obtained by integrating
485 information on the relationship between seismic Vs, soil mechanical resistance
486 and drilling observations into the mapping process. An analysis of the
487 correlation between seismic Vs and soil mechanical behaviours provided an
488 effective basis for the accurate delineation of a specific soil attribute. According
489 to the discussion, the analysis of the correlation between the seismic shear
490 wave velocity and the soil bulk density at an interface of strongly contrasted
491 mechanical properties should be studied further.
492 The future of precise mapping of selected soil properties using geophysical
493 seismic techniques in dependent on the understanding of relationships between
494 geophysical signals obtained from this technology and the overall spatial and
495 temporal variability of soil patterns. As the value of the soil resources and
496 associated ecological services receive greater recognition, digital soil mapping
497 based on seismic shear wave velocity can provide spatial data regarding soil
498 degradation that will serve as an essential tool for soil conservation and/or soil
499 rehabilitation.
500

501 **5. Acknowledgements**

502

This study was funded by the FP7-DIGISOIL project. The DIGISOIL project (FP7-ENV-2007-1 N°211523) is financed by the European Commission under the 7th Framework Programme for Research and Technological Development, Area "Environment", Activity 6.3 "Environmental Technologies". The authors thank J. F. Ouvry from AREAS for his help in focusing the study field and Alexis Rochat for his help in acquiring field seismic data. Finally, the authors thank the editors of *Geoderma* and two anonymous reviewers for their comments and suggestions that led to an improved version of the manuscript.

6. References

Afnor, Norme française NF XP P 94-105, Essai de pénétration dynamique à énergie variable, Association française de normalisation, 2000.

Azaria, A., C. Zelt, A. Levander, 2003. High-resolution seismic mapping at a groundwater contamination site: 3-D traveltime tomography of refraction data, EGS-AGU-EUG Joint Meeting, Nice, France.

Biot Y, Lu X.X. 1995. Loss of yield caused by soil erosion on sandy soils in the UK, Soil use and Management 11 (4)157-162.

Bremer E., Black M., Townley-Smith L., Malhi SS., Izaurralde RC., Larney FJ. 2008. SimPLE.ca: Simulator of productivity loss due to erosion for Canada, Canadian Journal of Soil Sciences 88 (3) 365-376.

524 Bullen, K. E., 1963, An introduction to the theory of seismology: Cambridge
525 Univ. Press.
526 Burgess, T., Webster, R., McBratney, A., 1981. Optimal interpolation and
527 isarithmic mapping of soil properties. IV. Sampling strategy. J. Soil Sci. 32,
528 643–659.
529 Burns, S.E., Mayne, P.W., 1996. Small and high-strain measurements of in-situ
530 soil properties using the seismic cone penetrometers. TRR 1548 Small-
531 Magnitude Measurements in Geotechnical Engineering. National Academy
532 Press, pp. 81-88.
533 J.B. Campbell and W.J. Edmonds, 1984. The missing geographic dimension to
534 soil taxonomy. Annals of the Association of American
535 Geographers, 74 (1984), pp. 83–97.
536 Cerdan O., G. Govers, Y. Le Bissonnais, K. Van Oost, J. Poesen, N. Saby, A.
537 Gobin, A. Vacca, J. Quinton, K. Auerswald, A. Klik, F.J.P.M. Kwaad, D.
538 Raclot, I. Ionita, J. Rejman, S. Rousseva, T. Muxart, M.J. Roxo, T. Dostal.
539 2010. The rate and spatial distribution of soil erosion in Europe,
540 Geomorphology 122, 167-177.
541 Chaplot, V., Walter, C., Curmi, P., Hollier-Larousse, A., 2001. Mapping field-
542 scale hydromorphic horizons using Radio-MT electrical resistivity.
543 Geoderma 102, 61–74.

544 Debeglia N., Bitri A., Thierry P., 2006. Karst investigations using microgravity
545 and MASW; Application to Orléans, France. *Near Surface Geophysics*, 4,
546 215-225.

547 Dikmen, U., 2009. Statistical correlations of shear wave velocity and penetration
548 resistance for soils. Journal of Geophysics and Engineering, volume 6,
549 number 1.

550 Eigenberg, R.A., Korthals, R.L., Neinaber, J.A., 1998. Geophysical
551 electromagnetic survey methods applied to agricultural waste sites. J.
552 Environ. Qual. 27, 215–219.

553 European Commission (2002). *Towards a strategy for soil protection*, COM
554 (2002) 179 final. Internet:http://europa.eu.int/comm/environment/
555 agriculture/soil_protection.htm.

556 European Commission. 2006. Thematic Strategy for Soil Protection,
557 COM(2006)231 final. Internet: http://eur-lex.europa.eu/LexUriServ/Lex
558 UriServ.do?uri=COM:2006:0231:FIN:EN:PDF

559 Foti, S., (2000) Multistation Methods for Geotechnical Characterization using
560 Surface-waves, Dottorato di Ricerca in Ingegneria Geotecnica.

561 Gourvès, R., Barjot, R., 1995. Le pénétromètre dynamique léger Panda.
562 Comptes rendus, 11ème congrès Européen de Mécanique des Sols et
563 des Travaux de Fondations, Copenhague, vol. 3, 83-88.

564 Grandjean G. and Bitri A., (2006) 2M-SASW: inversion of local Rayleigh wave
565 dispersion in laterally heterogeneous subsurfaces: application to Super-
566 Sauze landslide (France). Near Surface Geophysics,, 367-375.
567 Grandjean, G., 2006a. A seismic multi-approach method for characterizing
568 contaminated sites. J. Applied Geophys., 58, 87-98.
569 Grandjean G., 2006b. Imaging subsurface objects by seismic P-wave
570 tomography: numerical and experimental validations. Near Surface
571 Geophysics, 275-283.
572 Grandjean, G., Malet, J.P., Bitri, A., and Meric O., 2007. Geophysical data
573 fusion by fuzzy logic for imaging mechanical behaviour of mudslides. Bull.
574 Soc. Geol. France, 177, 2, 133-143.
575 Hadgu KM., Rossing WAH., Kooistra L., van Bruggen AHC. 2009. Spatial
576 variation in biodiversity, soil degradation and productivity in agricultural
577 landscapes in the highlands of Tigray, northern Ethiopia, Food Security 1
578 (1) 83-97.
579 Hasancebi, N. and Ulusay, R. (2006). “Empirical correlations between shear
580 wave velocity and penetration resistance for ground shaking assessments,”
581 *Bull Eng Geol Environ*, 66, 203-213.
582 Heckrath G, Djurhuus J, Quine TA, Van Oost K, Govers G, Zhang Y. 2005.
583 Tillage erosion and its effect on soil properties and crop yield in Denmark,
584 Journal of Envirnmental Quality 34 (1) 312-324.

585 Hermann, R.B., 1987. Computer programs in seismology. Saint-Luis University,
586 USA.
587 Imai, T. and Yoshimura, Y. (1975). “The relation of mechanical properties of
588 soils to P and S-wave velocities for ground in Japan,” *Technical Note,* OYO
589 Corporation.Iyisan, R. (1996). “Correlations between shear wave velocity
590 and in-situ penetration test results,” *Tech. J. Chamber Civil Eng. Turkey,* 7**,**
591 1187–99 (in Turkish).
592 Jafari, M. K., Shafiee, A. and Ramzkhah, A. (2002). “Dynamic properties of the
593 fine grained soils in south of Tehran,” *J. Seismol. Earthq. Eng.,* 4**,** 25–35.
594 Kachanoski, R.G., Gregorich, E.G., Van Wesenbeeck, J., 1988. Estimating
595 spatial variations of soil water content using noncontacting
596 electromagnetic inductive methods. Can. J. Soil Sci. 68, 715–722.
597 Kalinski, R.J., Kelly, W.E., 1993. Estimating water content of soils from electrical
598 resistivity. Geotech. Test. J. 16, 323–329.
599 Langton, D. D., 1999. The PANDA lightweight penetrometer for soil
600 investigation and monitoring material compaction, Ground Engineering.
601 Lanz, E., Mauer, H., Green, A.G., 1998. Refraction tomography over a buried
602 waste disposal site. Geophysics 63, 1414– 2007-02-21.
603 Lunne, P., Robertson, P. KK., and Powell, J. J. M., 1997, Cone penetration
604 testing in geotechnical practice. E and FN SPON.

Martin-Clouaire R., Cazemier D.R., Lagacherie P. 2000. Representing and processing uncertain soil information for mapping soil hydrological properties Computers and Electronics in Agriculture 29 (1-2), 41-57

Matheron, G., 1965. Les variables régionalisées et leur estimation: une application de la théorie de fonctions aléatoires aux sciences de la nature. Masson et Cie, Paris. 306 pp.

Mayne, P.W., 2001, Stress-strain-strength-flow parameters from enhanced in-situ tests, *Proceedings of the International Conference on In-Situ Measurement of Soil Properties and Case Histories, Bali, pp. 27-48.*

Mayne, P. W., Rix, G. J., Correlations between shear wave velocity and cone tip resistance in natural clays, Soil and Foundations 35 (1995) (2), pp. 107–110.

McMechan G. A., Yedlin M. J., 1981, Analysis of dispersive waves by wave field transformation. Geophysics vol. 46 p. 869-874.

Michot, D., Benderitter, Y., Dorigny, A., Nicoullaud, B., King, D., Tabbagh, A., 2003. Spatial and temporal monitoring of soil water content with an irrigated corn crop cover using electrical resistivity tomography. Water Resour. Res. 39, 11–38.

Miller, R.D., Xia, J., Park, C.B., and Ivanov, J.M., 1999, Multichannel analysis of surface waves to map bedrock: *The Leading Edge*, 18, 1392–1396.

Myers, D.E., 1994. Spatial interpolation: an overview. Geoderma 62, 17–28.

626 Nazarian, S., Stokoe,K. H., II, and Hudson,W. R., 1983, Use of spectral analysis
627 of surface waves method for determination of moduli and thicknesses of
628 pavement systems: Transport. Res. Record, **930**, 38– 45.
629 Papy F, Douyer C. 1991. Influence des états de surface du territoire agricole sur
630 le déclenchement des inondations catastrophiques. *Agronomie* **11**: 201–215.
631 Park, C.B., Miller, R.D., Xia, J., Ivanov, J., 2000. Multichannel seismic surface-
632 wave methods for geotechnical applications. Proc. of the First Int. Conf. on
633 the App. of Geophys. Methodologies to Transportation Facilities and
634 Infrastructure, St. Louis, December 11–15.
635 Park, C.B., Miller, R.D., and Xia, J., 1999a, Multimodal analysis of high
636 frequency surface waves: *Proceedings of the symposium on the*
637 *application of geophysics to engineering and environmental problems* '99,
638 115–121.
639 Park, C.B., Miller, R.D., and Xia, J., 1999b, Multichannel analysis of surface
640 waves: *Geophysics*, 64, 800–808.
641 Park, C. B., Xia, J., and Miller, R. D., 1998a, Ground roll as a tool to image
642 near-surface anomaly: 68th Ann. Internat. Mtg., Soc. Expl. Geophys., Expanded
643 Abstracts, 874–877.
644 Park, C. B., Xia, J., and Miller, R. D., 1998b, Imaging dispersion curves of
645 surface waves on multichannel record: 68th Ann. Internat. Mtg., Soc. Expl.
646 Geophys., Expanded Abstracts, 1377–1380.

Qi F., Zhu A-X. 2011. Comparing three methods for modeling the uncertainty in knowledge discovery from area-class soil maps Computers & Geosciences 37 (9), 1425-1436

Rejman J., I. Iglik. 2010. Topsoil reduction and cereal Yields on loess soils of Southeast Poland Land Degrad. Develop. 21: 401–405.

Richart, F. E., Hall, J. R., and Woods, R. D., 1970, Vibrations of soils and foundations: Prentice-Hall, Inc.

Rhoades, J.D., Corwin, D.L., 1981. Determining soil electrical conductivity-depth relations using inductive electromagnetic soil conductivity meter. Soil Sci. Soc. Am. J. 45, 255–260.

Rhoades, J.D., van Schilfgaarde, J., 1976. An electrical conductivity probe for determining soil salinity. Soil Sci. Soc. Am. J. 40, 647–651.

Robain, H., Descloitres, M., Ritz, M., Atangana, Q.Y., 1996. A multiscale electrical survey of a lateritic soil system in the rain forest of Cameroon. J. Appl. Geophys. 34, 237–253.

Samouëlian, A., Cousin, I., Tabbagh, A., Bruand, A., Richard, G., 2005. Electrical resistivity survey in soil science: a review. Soil Tillage Res. 83, 173–193.

Sanglerat. G, The penetrometer and soil exploration, Elsevier, 1975.

Stokoe, K. H., II, Wright, G. W., James, A. B., and Jose, M. R., 1994, Characterization of geotechnical sites by SASW method, *in*Woods, R. D., Ed., Geophysical characterization of sites: Oxford Publ.

669 Stuedlein, A. W., 2010. Shear-wave velocity correlations for Puyallup River
670 alluvium, J. Geotech. and Geoenvir. Engrg. 136, 1298 (2010);
671 doi:10.1061/(ASCE)GT.1943-5606.0000342 (7 pages)
672 Sturtevant, K. A., Baker, G. S., Snyder, C., Kopczynski, S., 2004.
673 Hydrogeophysical characterization of bedrock fracture orientations using
674 azimuthal seismic refraction tomography. AGU, H23A-1122.
675 Sykora, D. E. and Stokoe, K. H. (1983). "Correlations of in-situ measurements
676 in sands of shear wave velocity," *Soil Dyn. Earthq. Eng.,* 20**,** 125–36.
677 Sykora, D. W. and Koester, P. J. (1988). "Correlations between dynamic shear
678 resistance and standard penetration resistance in soils," *Earthq. Eng. Soil*
679 *Dyn.,* 2**,** 389–404.
680 Tarantola, A., 1987, Inverse problem theory. Elsevier Science Publishing Co.,
681 Inc.
682 Tengberg A, Stocking M, Dechen SCF. 1997. The impact of erosion on soil
683 productivity - An experimental design applied in Sao Paulo State, Brazil,
684 Geografiska Annaler Series A, Physical Geography 79A (1-2) 95-107.
685 Thompson, J.A., Bell, J.C., 1996. Color index for identifying hydric conditions for
686 seasonally saturated mollisols in Minnesota. Soil Sci. Soc. Am. J. 60,
687 1979–1988.
688 Ulugergerli, U. E. and Uyanik, O. (2007). "Statistical correlations between
689 seismic wave velocities and SPT blow counts and the relative density of
690 soils," *J. Test. Eval.,* 35**,** 1–5.

691 U.S. Department of Agriculture, 2003. National Soil Survey Handbook, title 430-
692 VI. [Online] Available: bhttp:// soils.usda.gov/technical/handbook/N.
693 Van-Camp. L., Bujarrabal, B., Gentile, A-R., Jones, R.J.A., Montanarella, L.,
694 Olazabal, C. and Selvaradjou, S-K. (2004). Reports of the Technical
695 Working Groups Established under the Thematic Strategy for Soil
696 Protection. EUR 21319 EN/1, 872 pp. Office for Official Publications of the
697 European Communities, Luxembourg.
698 Webb, TH, Lilburne, LR. 2005 Consequences of soil map unit uncertainty on
699 environmental risk assessment AUSTRALIAN JOURNAL OF SOIL
700 RESEARCH 43 (2), 119-126
701 Williams, B.G., Hoey, D., 1987. The use of electromagnetic induction to detect
702 the spatial variability in the salt and clay content of soils. Austr. J. Soil Res.
703 25, 21–27.
704 World Reference Base, 1998. World Reference Base for Soil Resources. FAO,
705 World Resources Report no. 84, Rome, Italy.
706 Xia, J., Miller, R.D., and Park, C.B., 1999, Configuration of near surface shear
707 wave velocity by inverting surface wave: *Proceedings of the symposium*
708 *on the application of geophysics to engineering and environmental*
709 *problems* '99, 95–104.
710 Ye L., Van Ranst E. 2009. Production scenarios and the effect of soil
711 degradation on long-term food security in China, Global Environmental
712 Change 19 464–481.

713 Zhou. S, Caractérisation des sols de surface à l'aide du pénétromètre
714 dynamique léger à énergie variable type Panda, thèse, université Blaise-
715 Pascal, Clermont-Ferrand-2, 1997, 179 p.
716

7. Tables

Table 1. Soil properties for 4 drilling observations along the n°5 transect with a spacing of 40 m in the middleslope and 20 m in the downslope (Figure 1). θ: water content, ρr: real density, ρb: bulk density, ThickLM: thickness of the loamy material horizon, Depth: sample depth, Depth Bis: replicate sample depth.

Table. 2. General statistics (Min: minimum; Max: maximum; Av: average; Median; Stdev, standard deviation; Var: variance; CV, coefficient of variation; Skwe, skewness; Kurt, kurtosis for *ThickLM*, which is the thickness of the loamy material horizon (m); *Qd*: the mechanical resistance (MPa).

8. Figure captions

Figure 1. Location of the study plot within the Bourville catchment in Normandy, a region of Northern France. Contour lines of absolute altitude with 0.5 m intervals within the 120×130 m plot are presented for the 157 data points of the seismic survey. Position of the 4 drilling events and the 12 penetrometer soundings are indicated along the n°5 transect.

Figure 2. Loamy sediments showing the critical thickness are rendered more vulnerable to runoff and water erosion relative to competent and nearly outcropping clays enriched with flints.

Figure 3. a) Photograph of the towing system with the seismic acquisition central and laptop computer. b) Photograph of the seismic array with 24 geophones regularly spaced at 50 cm. c) Schematic representation of the acquisition configuration with the key parameters: near offset *x0*, geophone spacing *Dx* and offset range *L*.

Figure. 4. Workflow diagram illustrating the methodology using to obtained reliable Vs versus depth models.

Figure 5. a) Example of recorded surface waves. b) Observed dispersion curve obtained by *Cf-f* domain transformation. c) Comparison between the initial and final Vs versus depth model obtained after the inversion step. d) Comparison between observed and synthetic dispersion curves. The relatively good fit between these curves indicates the reliability of the final model.

Figure 6. Qualitative comparison between a drilling observation, a penetrometer sounding and a Vs versus depth model at the same location. The relatively good correlations between Vs, mechanical properties of the soil and the observed lithologies are shown.

Figure 7. Representation of the Vs distribution. Two populations characterised by Gaussian laws of $mean_{1st\ layer}$ = 171 $m.s^{-1}$, $\sigma_{1st\ layer}$ = 80 $m.s^{-1}$and of $mean_{2nd\ layer}$ = 347 $m.s^{-1}$, $\sigma_{2nd\ layer}$ = 76 $m.s^{-1}$are distinguished.

Figure 8. Seismic and penetrometric sections along transect n°5. Threshold values of Vs=240 m/s and Qd=20 MPa overlay the sections in black dotted line and red solid line, respectively. Drilling observations overlay the seismic section in black crosses. There is a good agreement, in terms of *ThickLM*, between the threshold values and *ThickLM* obtained from drilling observations.

Figure. 9. Observed *Vs* after exclusion filtering (*Vs*>240 m/s) versus averaged interpolated *Qd* computed for the thicknesses of *Vs* intervals on 1D models along the n°5 transect.

Figure 10. a) Spatial variations in the thickness of the loamy material horizon (*ThickLM*) obtained using *MASW*. b) Spatial variations in the stiffness of the loamy material horizon (*StiffLM*) obtained using Eq. (2). Contour lines of absolute altitude with a 0.5 m interval overlay the map. The 4 drilling observations, 12 penetrometric data points and 157 seismic data points are shown on the map. The black dotted line represents the buried former gully that is visible in the photograph. c) Photograph showing the buried former gully.

Figure 11. a) Directional variogram of *ThickLM*. b) Directional variogram of *StiffLM.*

Figure 12. Plot of estimated ThickLM values obtained using the MASW methodology and the observed ThickLM for the 4 drilling observations.

Figure 1

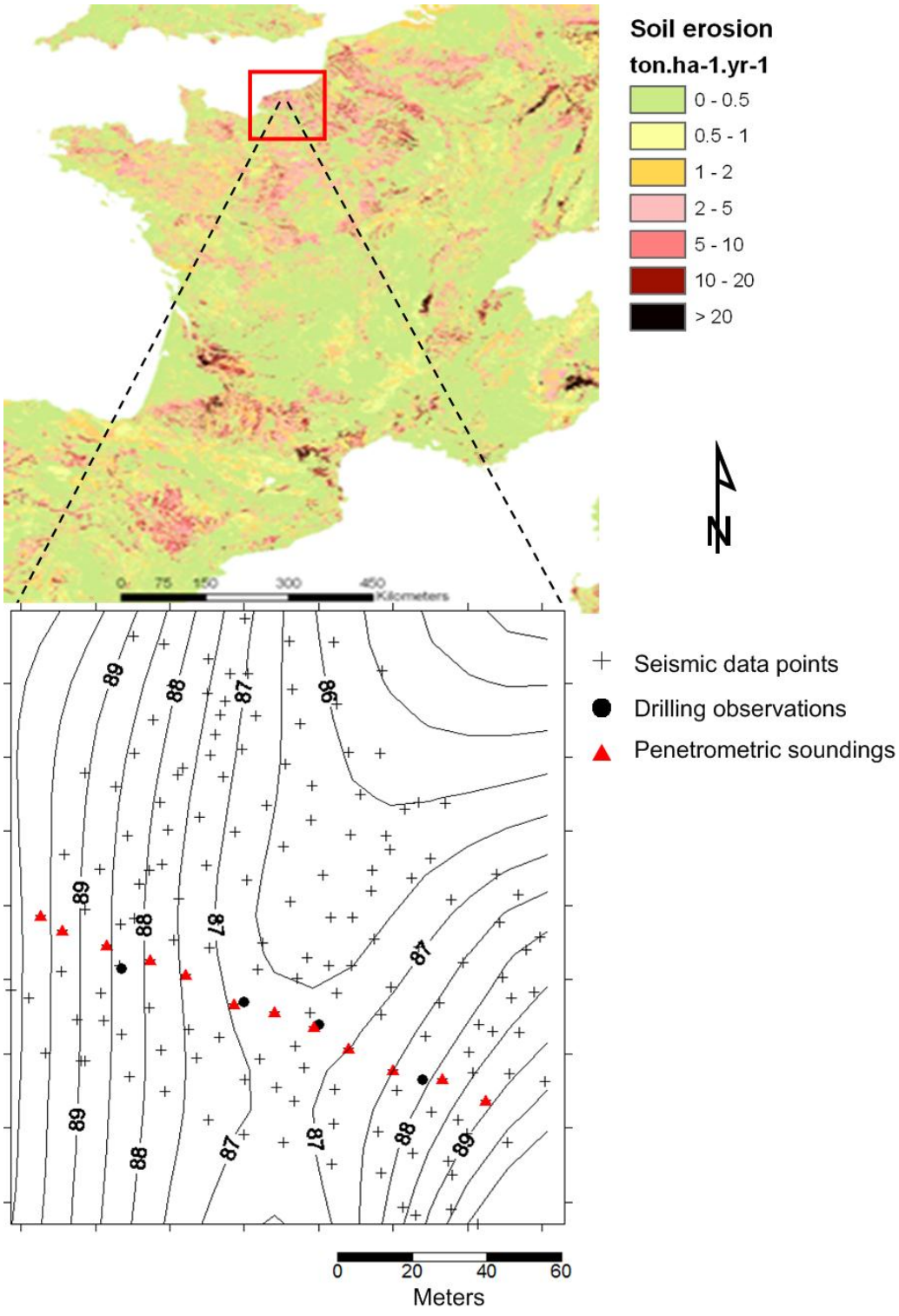
Soil erosion
ton.ha-1.yr-1
0 - 0.5
0.5 - 1
1 - 2
2 - 5
5 - 10
10 - 20
> 20
0 75 150 300 450
Kilometers
N
Seismic data points
Drilling observations
Penetrometric soundings
89
88
87
86
0 20 40 60
Meters

794 Figure 2

795

796

797 Figure 3

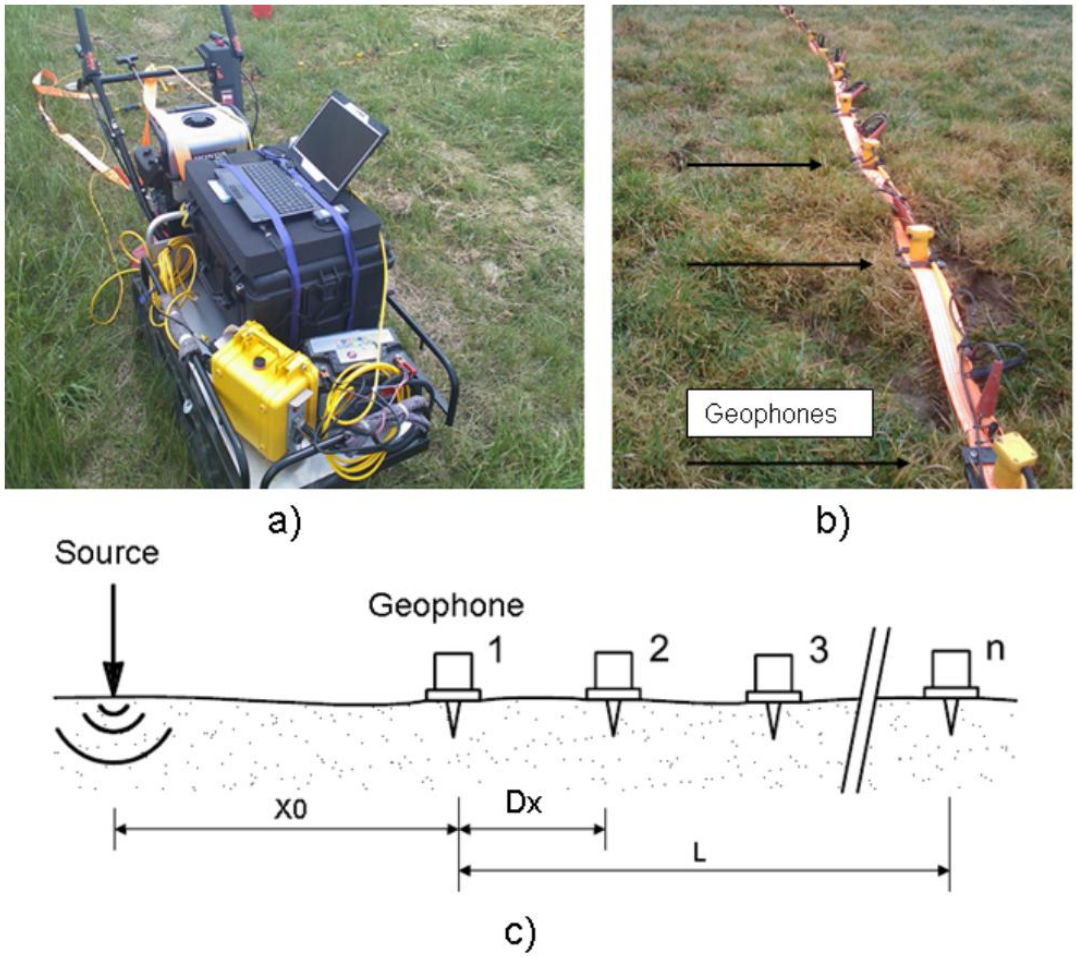

798

799

800 Figure 4

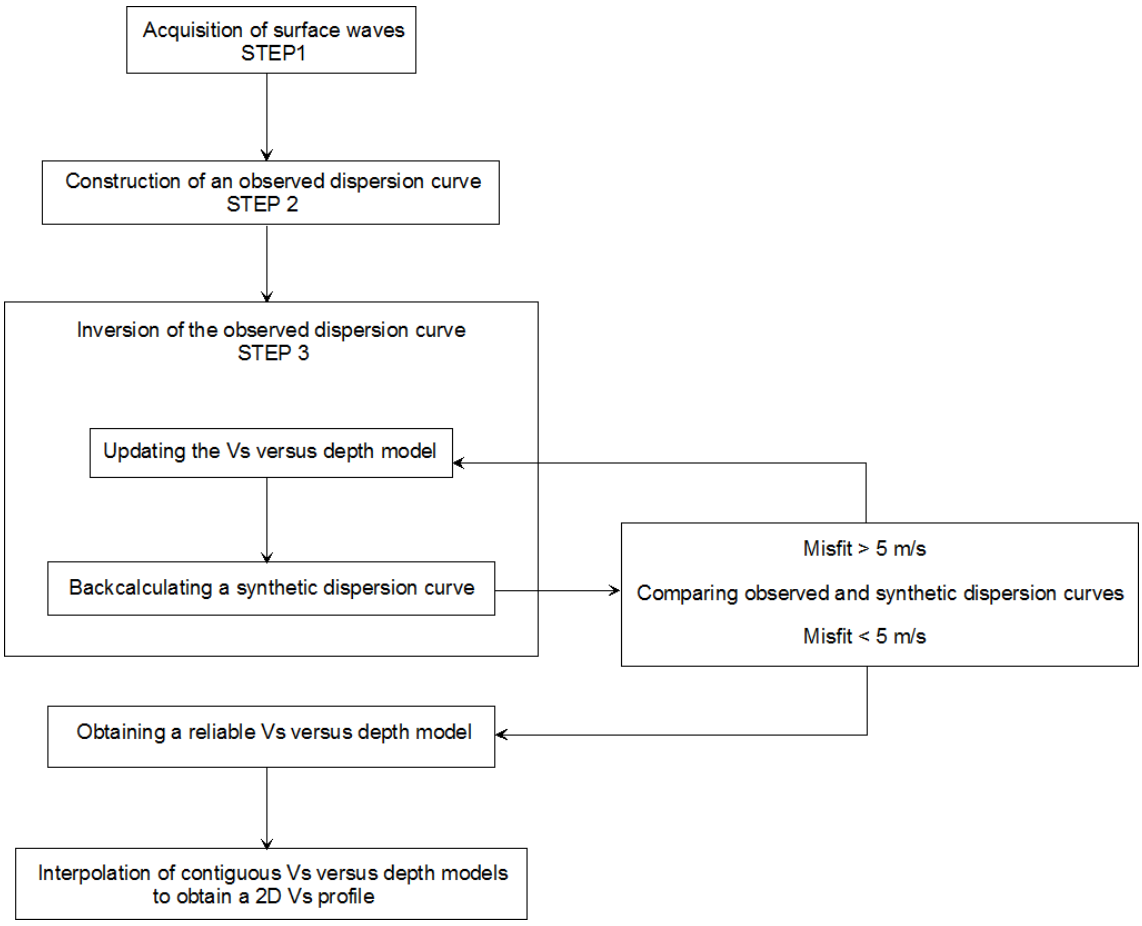

801

802

803 Figure 5

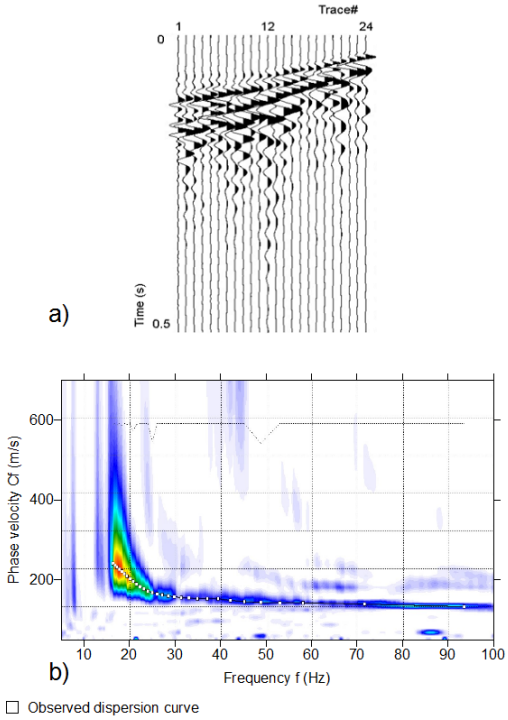

804

805

806 Figure 6

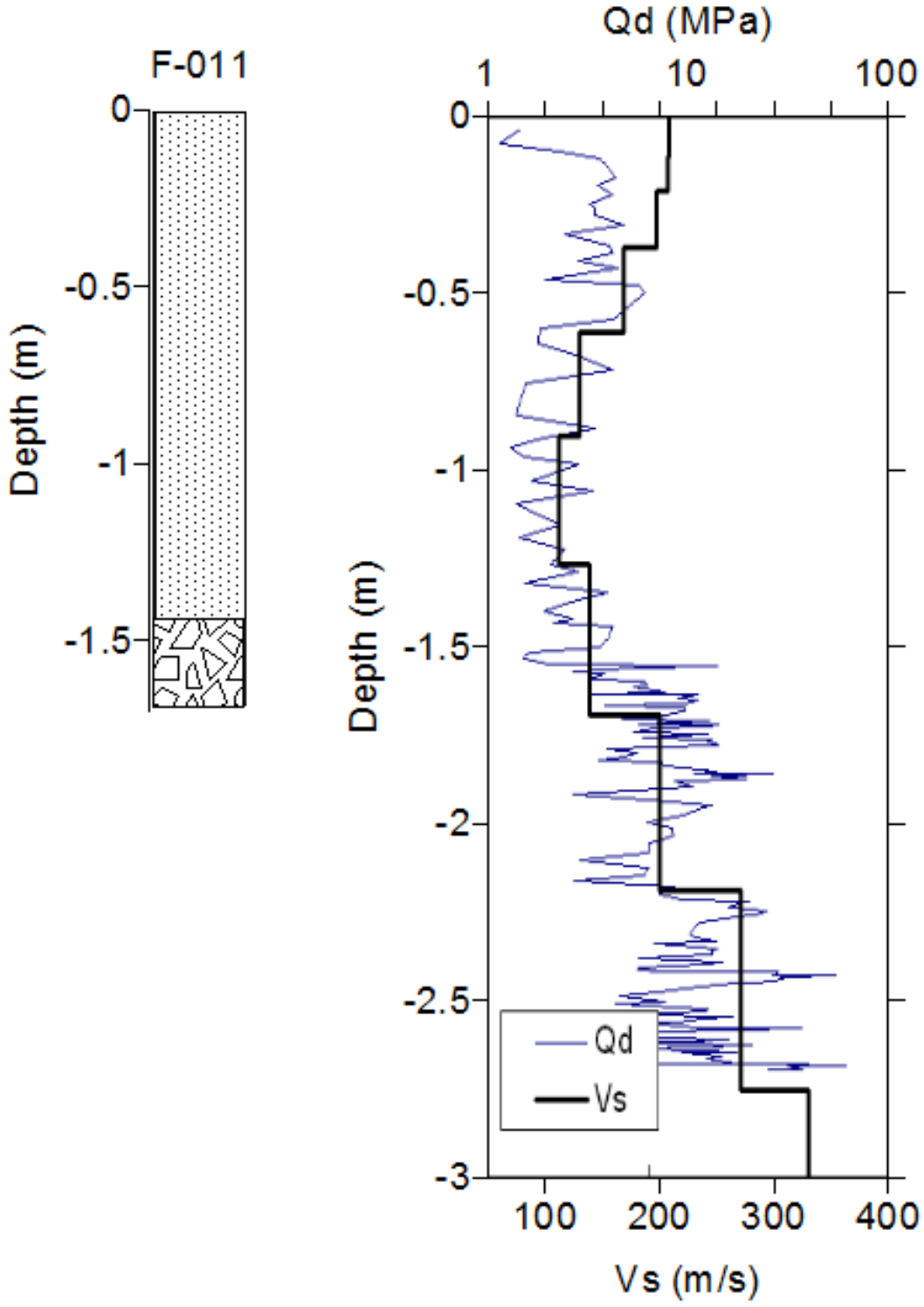

807

808

809 Figure 7

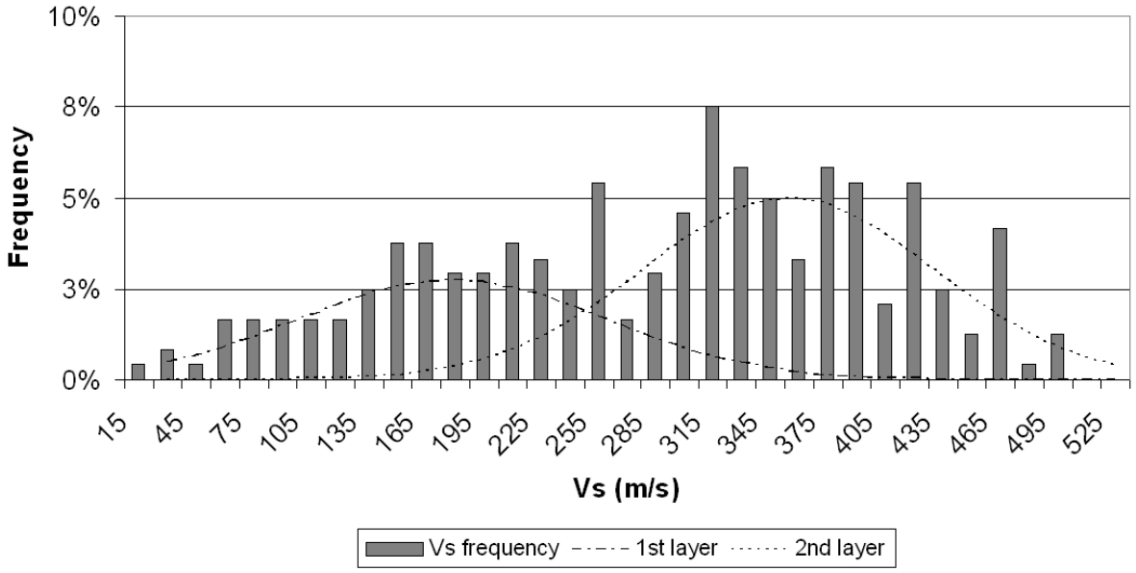

810

811

Figure 8

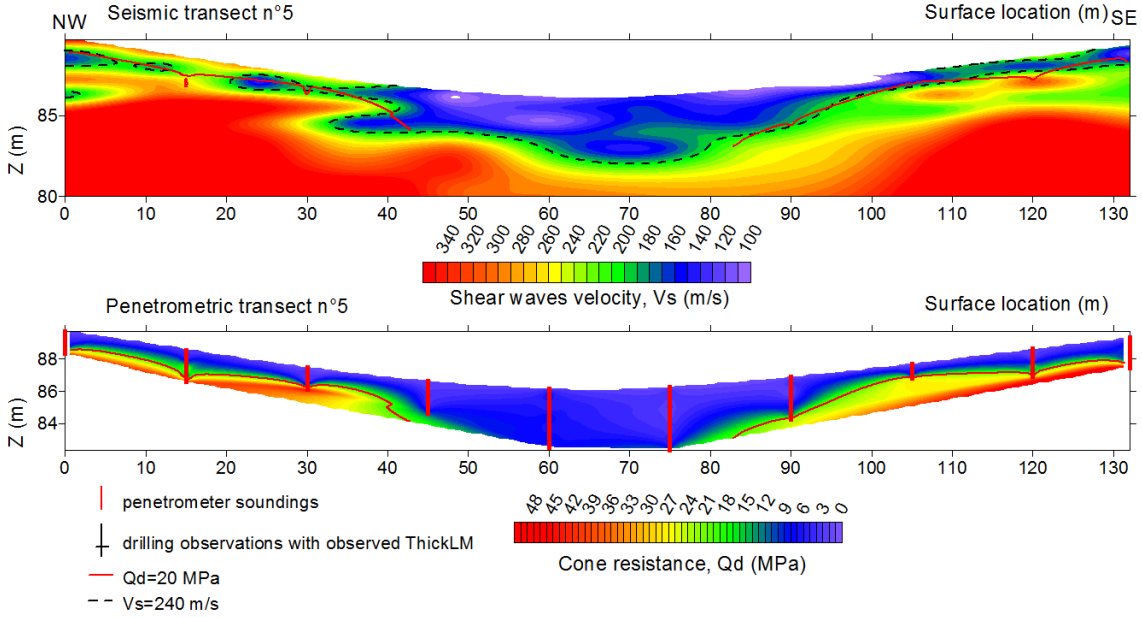
NW
Seismic transect n°5
Surface location (m)
SE
Z (m)
85
80
0 10 20 30 40 50 60 70 80 90 100 110 120 130
340 320 300 280 260 240 220 200 180 160 140 120 100
Shear waves velocity, Vs (m/s)
Penetrometric transect n°5
Surface location (m)
88
86
84
penetrometer soundings
drilling observations with observed ThickLM
Qd=20 MPa
Vs=240 m/s
48 45 42 39 36 33 30 27 24 21 18 15 12 9 6 3 0
Cone resistance, Qd (MPa)

815 Figure 9

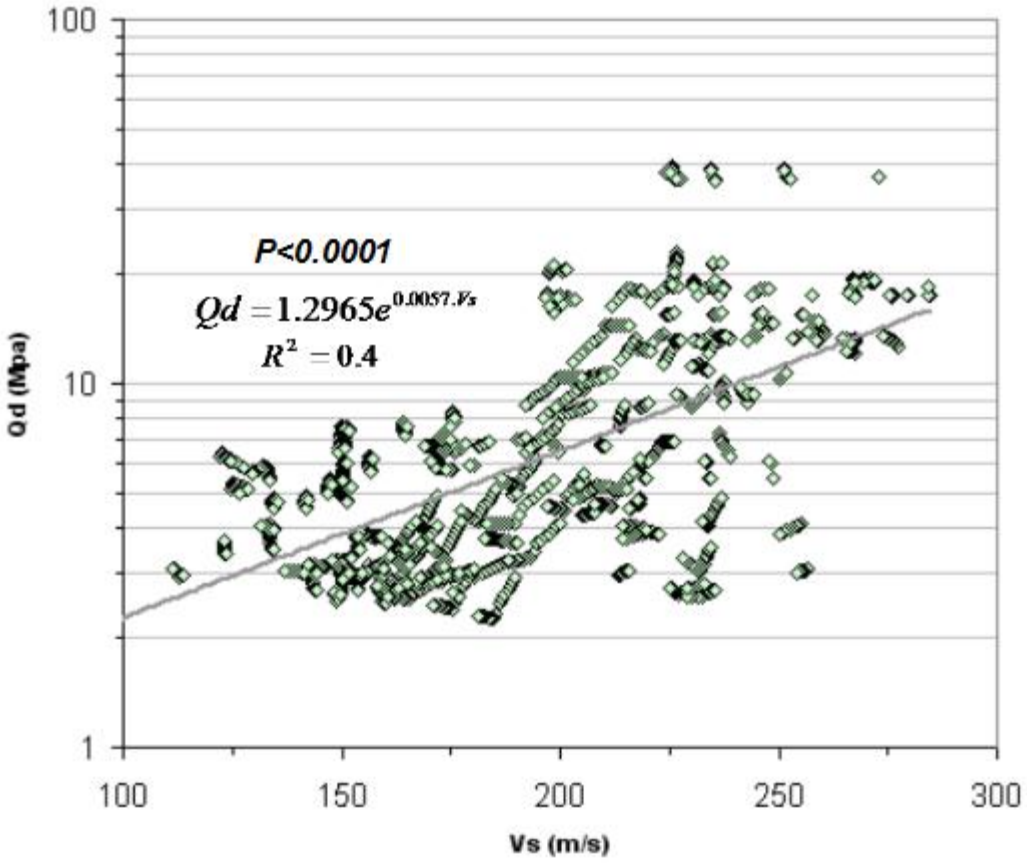

816

817

818 Figure 10

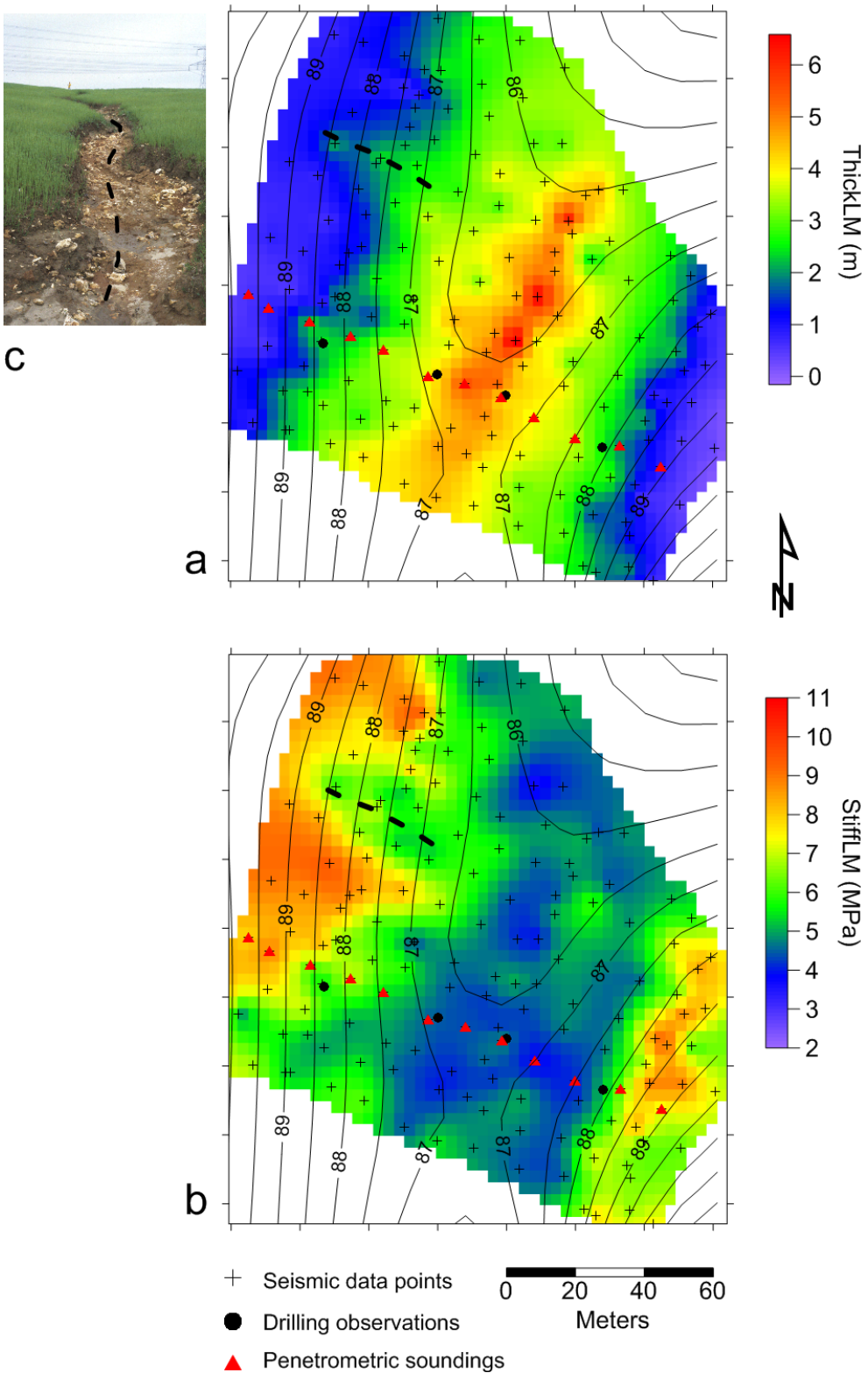

819

820

821 Figure 11

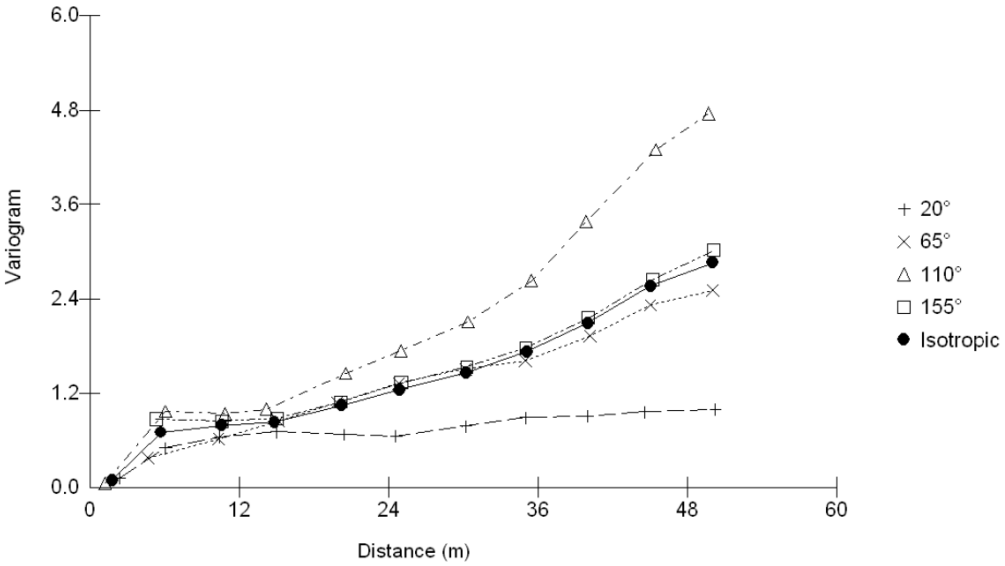

a

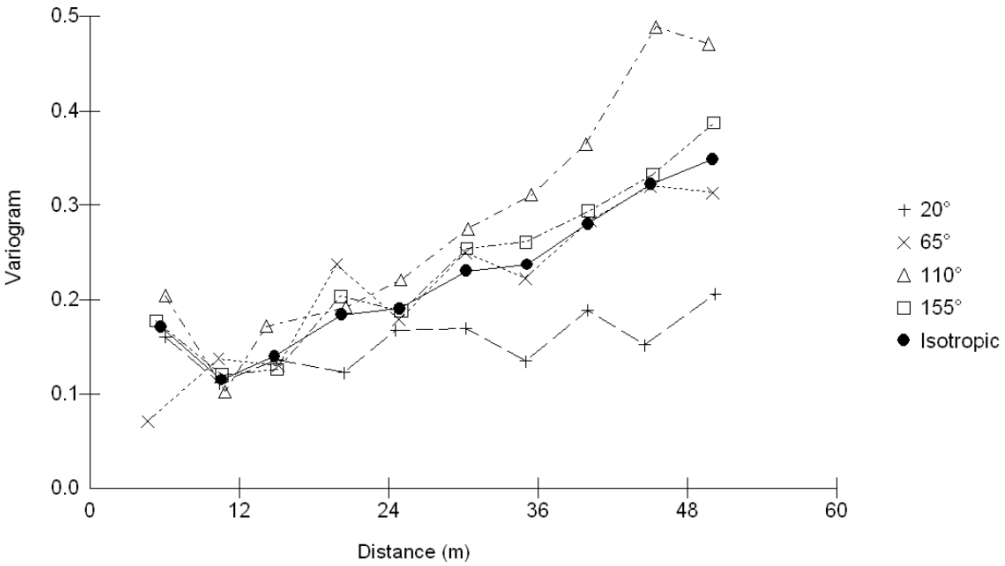

b

822

823

824 Figure 12

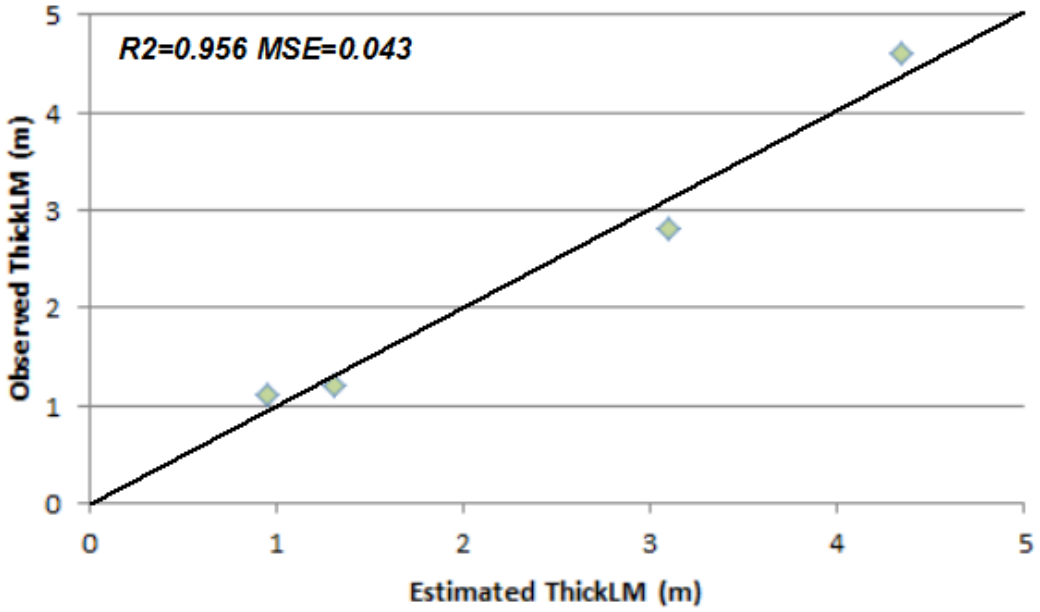

825